

Rh₂O₃(II)-type structures in Ga₂O₃ and In₂O₃ under high pressure: Experiment and theory

Hitoshi Yusa*

Advanced Nano Materials Laboratory, National Institute for Materials Science, 1-1 Namiki, Tsukuba, Ibaraki 305-0044, Japan

Taku Tsuchiya†

Geodynamics Research Center, Ehime University, 2-5 Bunkyo-cho, Matsuyama 790-8577, Japan

Nagayoshi Sata‡

Institute for Frontier Research on Earth Evolution, Japan Agency for Marine-Earth Science and Technology, 2-15, Natsushima-cho, Yokosuka, 237-0061, Kanagawa, Japan

Yasuo Ohishi§

Japan Synchrotron Radiation Research Institute, 1-1-1 Kouto, Sayo-cho, 679-5198, Hyogo, Japan

(Received 19 July 2007; published 15 February 2008)

High-pressure transitions of Ga₂O₃ and In₂O₃ were examined by using a laser-heated diamond-anvil cell combined with *in situ* x-ray diffractometry at pressures up to 108 GPa and 20 GPa, respectively. To predict the transition pressure to high-pressure phases, first principles static lattice energy calculations based on the density functional theory were also performed. Rh₂O₃(II) phases were confirmed as post corundum phases for both Ga₂O₃ and In₂O₃ at about 37 GPa and 7 GPa, respectively. The transition pressures determined by high-pressure experiments are almost consistent with those by theoretical computations. In regard to the present sesquioxides, a link of transition from corundum to perovskite was not confirmed. The Rh₂O₃(II) phases converted to corundum phases under decompression at room temperature. The bulk modulus of Rh₂O₃(II) phase in Ga₂O₃ and In₂O₃ were determined as 271 ± 10 GPa and 169 ± 4 GPa with their pressure derivatives fixed at 4, respectively.

DOI: [10.1103/PhysRevB.77.064107](https://doi.org/10.1103/PhysRevB.77.064107)

PACS number(s): 61.05.C-, 61.50.Ks, 62.50.-p, 61.50.Ah

I. INTRODUCTION

Group-IIIB sesquioxides, such as gallium oxide and indium oxide, have been widely surveyed as attractive semiconductive materials with a wide band gap. Especially, their most stable phases at ambient condition, monoclinic β -Ga₂O₃ ($E_g=4.9$ eV) and cubic In₂O₃ ($E_g=3.7$ eV) (a bixbyte-type structure, i.e., a so-called C-rare-earth sesquioxide structure, denoted as C-RES hereafter), are promising materials for transparent electronic devices.¹⁻⁴ It has been reported that their dense phase is a corundum structure.⁵⁻⁸ The corundum structure of gallium sesquioxides (α -Ga₂O₃) can be generally prepared from β -Ga₂O₃ by high pressure and temperature synthesis at 4.4 GPa and 1000 °C.^{5,6} At ambient pressure, α -Ga₂O₃ is thermodynamically metastable and reverts to β -Ga₂O₃ at 600 °C.⁵ A few high-pressure experiments on Ga₂O₃ by x-ray, Raman, and fluorescence measurements have been done by diamond-anvil cell (DAC) under room-temperature compression.⁹⁻¹² The fluorescence shift of Cr³⁺-doped β -Ga₂O₃ is more sensitive to pressure than that of ruby; it is therefore expected to be used for a pressure sensor, especially in the low-temperature region.⁹ There is a contradiction in the x-ray-diffraction studies done on Ga₂O₃.¹⁰⁻¹² That is, the appearance of the tetragonal phase at approximately 13.3 GPa suggested by the former experiments¹⁰ was not reproduced by the latter experiments.¹¹ Instead, they indicated that β to α transition occurs at a pressure of 20 to 22 GPa under room temperature. As compared to high-pressure experiments under high temperature,^{5,6} the transition pressure is very high. It is thus thought that the discrepancy is caused by a kinetic problem

at room temperature, where significantly broadened diffraction peaks imply a structural disorder up to 38 GPa. Another high-pressure x-ray study was done on compression of the nanocrystalline Ga₂O₃ particles embedded in a glassy matrix at room temperature by DAC.¹² In this study, the transition of β to α was initiated at 6 GPa. However, even at 15 GPa, the transition was not completed.

The corundum structure of In₂O₃ was obtained by static,^{7,8} and dynamic compressions¹³ from the C-RES phase of In₂O₃. The lowest transition pressure was determined by static compression experiments at 6.5 GPa at 1000 °C.^{7,8} The stable pressure range of corundum was confirmed to be 15 to 25 GPa by a shock compression experiment.¹³ Apart from high-pressure syntheses, nowadays, ambient-pressure synthesis of corundum-type In₂O₃ has also been developed.¹⁴⁻¹⁶ It can be successfully achieved at low temperature (250 to 500 °C) in spite of the metastability of corundum-type In₂O₃. Although, as noted above, there are a lot of works on the synthesis of corundum phase in Ga₂O₃ and In₂O₃, an attempt to find the high-pressure phase of the corundum structure has not been tried yet. However, the high-pressure transitions of α -Al₂O₃ (corundum), so-called “post-corundum phase,” has attracted much attention from both theoretical¹⁷⁻²¹ and experimental high-pressure studies^{22,23} over the past twenty years. For instance, the post-corundum phase influences the utilization of ruby (Cr³⁺-doped α -Al₂O₃) pressure scale. Other than group-IIIB oxides, it is known that corundum is stable in the case of various sesquioxides such as Fe₂O₃, Cr₂O₃, V₂O₃, and Ti₂O₃ at ambient pressure.²⁴ Among sesquioxides, the postphase of hematite (Fe₂O₃) has been actively studied for its signifi-

cance in the Earth's interior.^{25–28} As a result of *in situ* high-pressure experiments using a laser heated DAC, it is reported that corundum (Al_2O_3) and hematite (Fe_2O_3) transform to a $\text{Rh}_2\text{O}_3(\text{II})$ -type structure at 96 GPa (Ref. 23) and to an orthorhombic perovskite (GdFeO_3 -type) or $\text{Rh}_2\text{O}_3(\text{II})$ -type structure at 30 GPa,²⁸ respectively. In these studies, the postcorundum phases could not be recovered at ambient pressure. *In situ* experiments were therefore indispensable for the discovery of these phases.

In the present study, to clarify the postcorundum phases in Ga_2O_3 and In_2O_3 as well as the high-temperature behavior of $\beta\text{-Ga}_2\text{O}_3$ and C-RES In_2O_3 , we conducted *in situ* x-ray-diffraction experiments under high pressure and temperature. Theoretical computations of the phase stability of their postcorundum candidates, such as $\text{Rh}_2\text{O}_3(\text{II})$ and orthorhombic perovskite, were also performed in order to predict the transition pressure in advance of the high-pressure experiments.

II. EXPERIMENTAL AND COMPUTATIONAL PROCEDURES

A. High-pressure experiments

Reagent-grade gallium oxide (99.999% pure) and indium oxide (99.999% pure) were used for the high-pressure experiments after preheating at 700 °C for 6 h in air. These structures were confirmed to be monoclinic $\beta\text{-Ga}_2\text{O}_3$ and cubic C-RES In_2O_3 by x-ray diffractometer under ambient temperature, respectively. The powder-form samples mixed with a small amount of platinum or gold powder, for enhancing heat by lasers, were put into a hole in a rhenium gasket seated on a diamond anvil. A few small grains of ruby pressure marker were also enclosed in the hole. To avoid the x-ray peaks overlapping with that from the samples, no pressure medium was used. The high-pressure x-ray powder diffraction experiments were performed at BL10XU in SPring-8. A symmetrical DAC was used for double sided heating. The samples were heated by Nd:YLF or Nd:YAG laser beam (20 microns or 60 microns in diameter) after being compressed to the target pressure. The temperature was monitored by spectroscopic measurements of emitted radiations from the samples during heating.²⁹ A monochromatic x-ray (30 keV) was collimated to 20 microns in diameter on the sample. The uncertainties in temperature within the 20 microns area was about $\pm 10\%$.³⁰ Debye rings from diffracted x-rays were detected by an imaging plate (IP) and a charge-coupled device (CCD). Conversion from the Debye rings to one-dimensional x-ray profiles versus 2θ was done by a computer program (Fit2D).³¹ A ruby-pressure scale was used for determining the pressure of the sample.³² We have confirmed no reaction of ruby markers with samples, since the recovered ruby markers indicated the standard ruby fluorescence spectra after the removal of residual strain by annealing at 500 °C for 5 h at atmospheric pressure. In case that the platinum's or gold's reflections did not overlap with sample's reflections; the pressure was cross-checked with the platinum or gold pressure scale.³³ Only the platinum scale was used for the pressure determination higher than 90 GPa.

B. Computational methods and results

Computations were performed within the density functional theory³⁴ (DFT) and the local density approximation

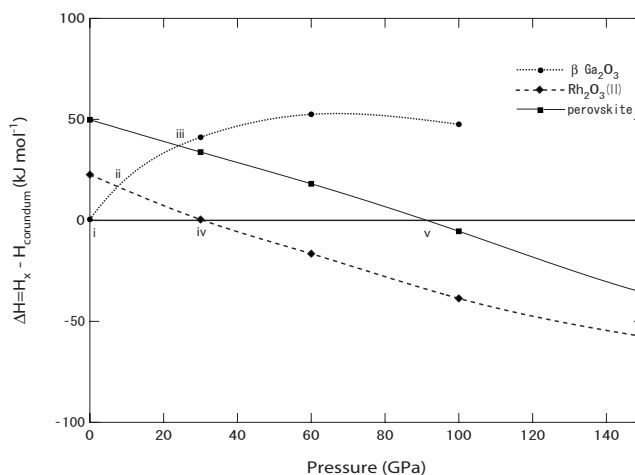


FIG. 1. Enthalpy differences relative to corundum for $\beta\text{-Ga}_2\text{O}_3$ (dotted line), $\text{Rh}_2\text{O}_3(\text{II})$ (dashed line), and perovskite (thin line) in Ga_2O_3 as a function of pressure under a static condition. There are five enthalpy crossovers corresponding to $\beta\text{-Ga}_2\text{O}_3$ –corundum (i), $\beta\text{-Ga}_2\text{O}_3$ – $\text{Rh}_2\text{O}_3(\text{II})$ (ii), $\beta\text{-Ga}_2\text{O}_3$ –perovskite (iii), corundum– $\text{Rh}_2\text{O}_3(\text{II})$ (iv), and corundum–perovskite (v).

(LDA).^{35,36} Ultrasoft pseudopotentials for gallium, indium, and oxygen were generated non-empirically using the methods of Vanderbilt.³⁷ The plane-wave cutoff was chosen as 50 Ry, and the irreducible parts of the Brillouin zone were sampled on $4 \times 4 \times 2$ (4 points), $2 \times 6 \times 4$ (12 points), $2 \times 2 \times 2$ (2 points), $4 \times 4 \times 2$ (6 points), and $4 \times 4 \times 2$ (4 points) Monkhorst-Pack meshes³⁸ for corundum, $\beta\text{-Ga}_2\text{O}_3$, C-RES In_2O_3 , $\text{Rh}_2\text{O}_3(\text{II})$ -type structures and orthorhombic perovskite, respectively. Structures were optimized using the variable cell-shape constant-pressure damped molecular dynamics technique³⁹ using the PWSCF code⁴⁰ until residual forces became less than 1.0×10^{-5} Ry/au. The effects of using a larger cutoff and a greater number of k points on the calculated properties were found to be insignificant.

Relative differences in static enthalpy ($T=0$ K) for corundum-type Ga_2O_3 are plotted in Fig. 1 as a function of pressure. The figure shows five enthalpy crossovers. Two crossovers are represented by the postcorundum transitions, corundum– $\text{Rh}_2\text{O}_3(\text{II})$ transition and the corundum–perovskite transition in Ga_2O_3 , which occur at 30 GPa (iv) and 91 GPa (v), respectively. Since no crossover is located between $\text{Rh}_2\text{O}_3(\text{II})$ and the perovskite phase in the calculated pressure range, the presence of the $\text{Rh}_2\text{O}_3(\text{II})$ stability field makes it difficult to convert to the perovskite phase. The most probable phase transformed from $\beta\text{-Ga}_2\text{O}_3$ at the lowest pressure is corundum at 0 GPa (i), as compared to the transitions to $\text{Rh}_2\text{O}_3(\text{II})$ at 7.5 GPa (ii) and perovskite at 24 GPa (iii).

The enthalpy differences for corundum-type In_2O_3 are plotted in Fig. 2. In total, five crossover points are found. The three crossovers, which are related to the C-RES–corundum– $\text{Rh}_2\text{O}_3(\text{II})$ transitions (i) to (iii), are densely located at 6 to 10 GPa. If we take an in-depth look around the pressure, the C-RES– $\text{Rh}_2\text{O}_3(\text{II})$ transition would appear prior to C-RES–corundum transition with increasing pressure. This means that the C-RES phase in In_2O_3 prefers $\text{Rh}_2\text{O}_3(\text{II})$

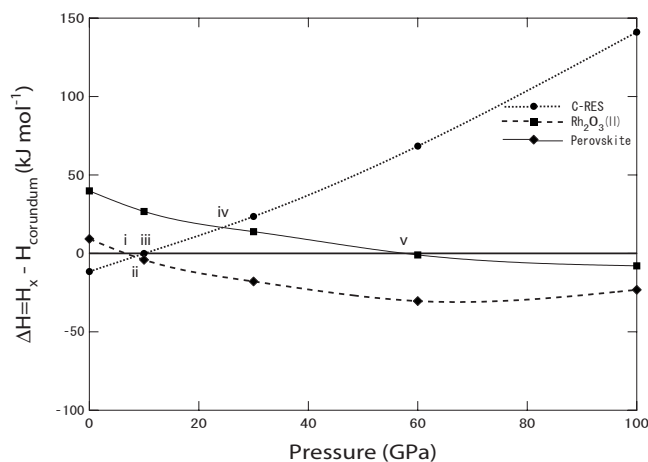


FIG. 2. Enthalpy differences relative to corundum for C-RES (dotted line), Rh₂O₃(II) (dashed line), and perovskite (thin line) in In₂O₃ as a function of pressure under a static condition. There are five enthalpy crossovers corresponding to corundum–Rh₂O₃(II) (i), C-RES–Rh₂O₃(II) (ii), C-RES–corundum (iii), C-RES–perovskite (iv), and corundum–perovskite (v).

to corundum as the transition phase. No crossover point between Rh₂O₃(II) and perovskite was found in In₂O₃ as well as in Ga₂O₃. The computation results also suggest that the C-RES–perovskite transition and corundum–perovskite transition takes place at 24 GPa (iv) and 57 GPa (v), respectively, if the Rh₂O₃(II) phase did not appear. In this study, calculations are all static ($T=0$ K), while the phase transitions are experimentally observed at high temperatures. Therefore, we are trying just qualitative comparison of the calculated and experimental transition pressures. Further computation results including temperature effects will be reported separately.⁴¹

III. EXPERIMENTAL RESULTS AND DISCUSSIONS

A. Rh₂O₃(II) structure in Ga₂O₃

Using examples from DFT-LDA computations, first, to examine the Rh₂O₃(II) structure in Ga₂O₃, we set the target pressure beyond 50 GPa. The sample was compressed up to 65 GPa at room temperature. In a previous study,¹¹ a pressure-induced transition to α -Ga₂O₃ was suggested by a room-temperature compression above 20 GPa. However, the present x-ray diffraction pattern of β -Ga₂O₃ changes to an unidentified broad diffraction pattern [Fig. 3(b)], which is apparently different from the α -Ga₂O₃. After the laser heating at 2300 ± 200 K for 15 min, the diffraction pattern changed to sharp peaks [Fig. 3(c)], and then the pressure drops to 52 GPa due to annealing effects under high temperature. As far as we know, the nonhydrostaticity in the annealed sample without a pressure medium is comparable with that in the nonannealed sample with a pressure medium. Therefore, we guess that the above discrepancy is not simply caused by a nonhydrostaticity but mostly by kinetics. The observed d values can be indexed by the orthorhombic structure of a space group of $Pbna$. The lattice parameters are set to $a=4.731(1)$ Å, $b=4.855(1)$ Å, and $c=6.942(2)$ Å by the

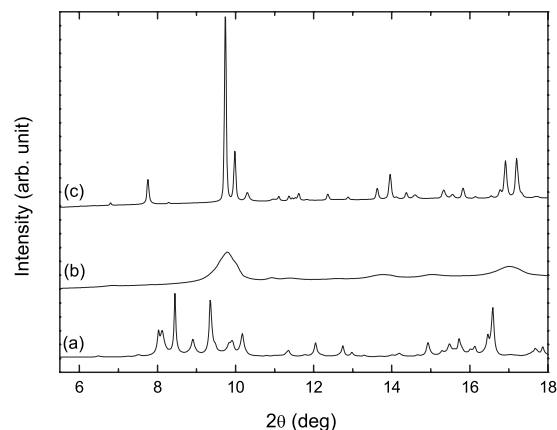


FIG. 3. X-ray diffraction profiles from Ga₂O₃ samples: (a) Starting β -Ga₂O₃ at ambient pressure, (b) at 65.0 GPa before laser heating, and (c) at 52.0 GPa after laser heating. All data were collected by IP.

least-square calculation. Recently, that the similarity between the diffraction patterns of orthorhombic perovskite structure ($Pbnm$) and Rh₂O₃(II) structure has been frequently reported.^{22,23,26,28,42} Hence, Rietveld refinement by the GSAS package⁴³ was performed on the basis of both perovskite and Rh₂O₃(II) structures (Fig. 4). As a whole, the discrepancy between observed and fitted profiles is small in both cases ($R_{wp}=0.07$ to 0.08). If a perovskite structure adopted, however, there are some local disagreements such as the absence of (110) reflection of $Pbnm$ perovskite [Fig. 4(a)], and a large fitting errors at $2\theta=15^\circ$ to 16° [Fig. 4(c)]. Moreover, according to DFT-LDA computation, if corundum to perovskite transition exists, the transition pressure would be located around 86 GPa, which is much higher than the pressure in the present experiments. Final refinements of the lattice parameters and the atomic coordinates as Rh₂O₃(II) are summarized in Table I. Figure 5(a) shows a crystallographic drawing of Rh₂O₃(II) based on the determined atomic coordinates. The drawings of α -Ga₂O₃ done by using reported crystal data⁶ is shown in Fig. 5(b) with a specific direction for comparison. A twinlike relation between Rh₂O₃(II) and corundum phase can be seen in the vertical direction in such crystallographic views. Considering the structural resemblance between Rh₂O₃(II) and corundum, which was already suggested by Shannon and Prewitt (1970),⁴² we conclude that the Rh₂O₃(II) structure is appropriate for the postcorundum phase in Ga₂O₃. The sample was gradually decompressed to ambient pressure at room temperature. During decompression from 32 to 21 GPa, the diffraction pattern changed to the corundum structure (Fig. 6). At the same time, peak broadening due to defects probably derived from the Rh₂O₃(II) structure was observed. The corundum phase was untransformed to β -Ga₂O₃ after decompression to ambient pressure.

B. Transition pressure of corundum to Rh₂O₃(II) in Ga₂O₃

To determine the transition pressure from corundum to Rh₂O₃(II), we repeatedly conducted high P - T experiments.

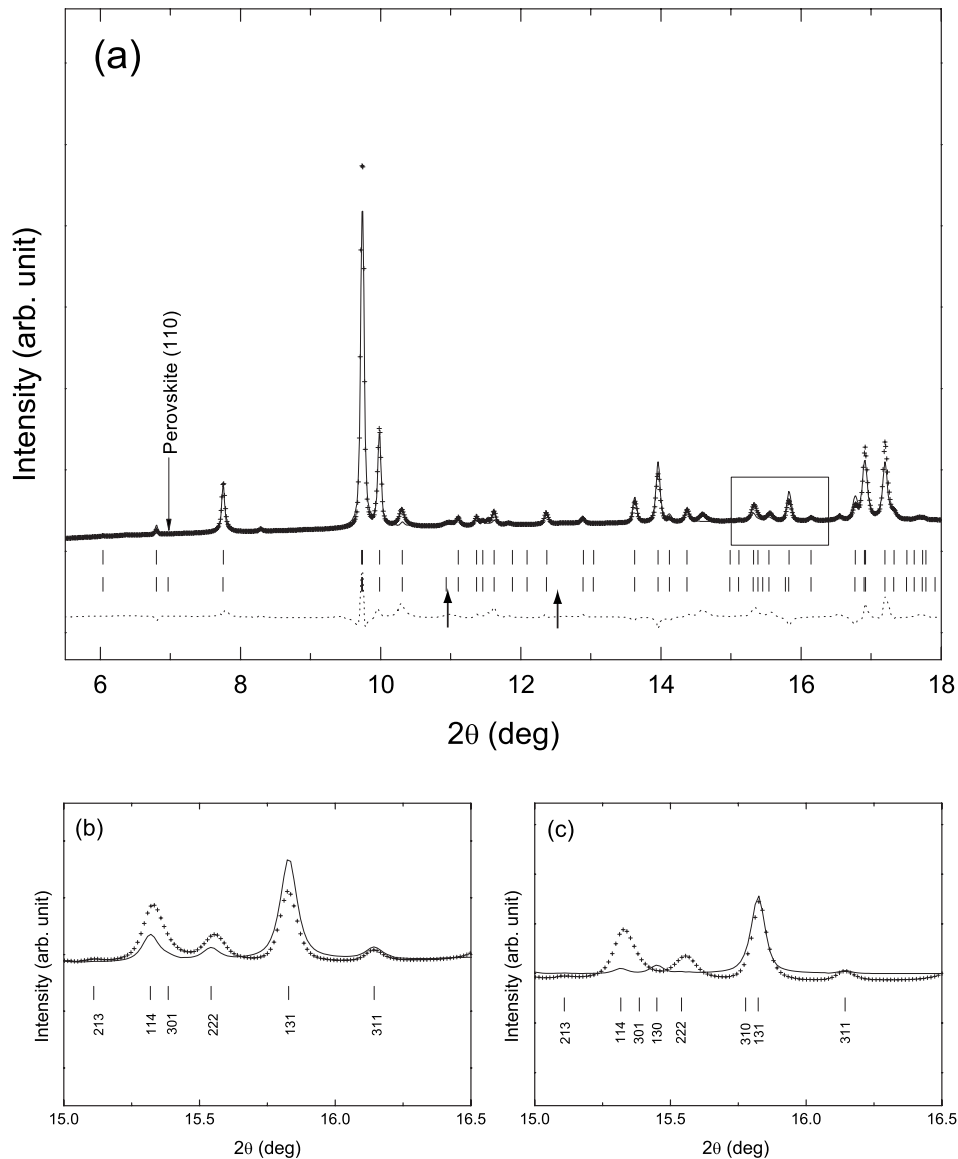


FIG. 4. Powder x-ray diffraction patterns obtained by the Rietveld method (GSAS). The observed pattern (crosses) is the same as that in Fig. 3(b). The difference (dotted line) between the observed and fitted pattern (thin line) is also shown on the same scale. Background was subtracted. Tick marks represent the calculated positions of the diffraction peaks of the $\text{Rh}_2\text{O}_3(\text{II})$ phase (upper) and orthorhombic perovskite (lower). Arrows indicate the position of platinum's reflections. The pressure determined from platinum (111) exhibits 51.5 GPa. (b) Enlargement of the square part in (a) fitted by $\text{Rh}_2\text{O}_3(\text{II})$ and (c) fitted by orthorhombic perovskite structure.

Since the $\text{Rh}_2\text{O}_3(\text{II})$ -type structure appears again at 47 GPa after laser heating at 1400–1750 K, the heating experiments continued with pressure, gradually released until the transition occurs (Fig. 7). No change was observed up to 38.5 GPa. The corundum phase began to appear at 36.2 GPa after heating at 1900–2150 K and increased to 50% in volume at 35 GPa. The volume fraction of corundum decreased

TABLE I. Refined atomic coordinates and lattice parameters determined by Rietveld analysis of the $\text{Rh}_2\text{O}_3(\text{II})$ phase ($Pbna$; $Z=4$) in Ga_2O_3 at 52.0 GPa.

Atom	x	y	z	U_{iso}^a
Ga	0.75004	0.04065	0.11292	0.0059
O1	0.63394	0.12120	0.85188	0.0092
O2	0.04173	0.25	0	0.0092
Lattice parameters	$a=4.732 \text{ \AA}$	$b=4.855 \text{ \AA}$	$c=6.942 \text{ \AA}$	$R_{\text{wp}}=0.077$

^aThe values from $\alpha\text{-Ga}_2\text{O}_3$ (Ref. 6) are used.

when it was reheated at 39 GPa. As a result, the transition boundary is located around 37 GPa at high temperature, i.e., 2000 ± 100 K. This result is consistent with 30 GPa from DFT-LDA computations (Fig. 1), particularly if considering that LDA usually underestimates the transition pressure by 5–10 GPa.^{21,41} The density increase can be calculated by applying the multiple phase analysis of the GSAS program to the diffraction pattern containing both phases. At 36.2 GPa, the density change is 2.3%, which is almost consistent with the 3.2% in the case of corundum– $\text{Rh}_2\text{O}_3(\text{II})$ transition in Rh_2O_3 at ambient pressure.⁴² We also investigated the post phase of $\text{Rh}_2\text{O}_3(\text{II})$ in Ga_2O_3 at high temperature beyond 100 GPa. However, we could not find any new phase up to 108 GPa and 2000 to 2500 K.

C. β - α transition in Ga_2O_3

Although the corundum phase is quenched at atmospheric pressure, it is known that the corundum is a metastable phase at high temperature. Heating at 600 °C makes it convert to

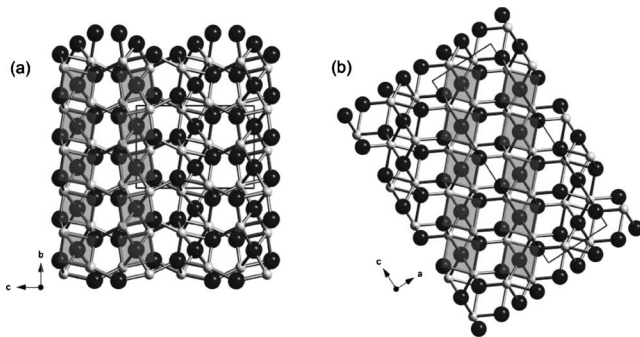


FIG. 5. (a) Projections of the Rh₂O₃(II) structures along the *a* axis and (b) the corundum structure along the hexagonal *a* axis in Ga₂O₃. The unit cell is indicated by the solid lines. The columns shown by the shaded area explain the twinlike relation between corundum and Rh₂O₃(II) structure.

β -Ga₂O₃.⁵ However, the transition pressure of β -Ga₂O₃ to corundum in equilibrium condition has not been determined. Under high *P-T* experimental condition, the crystal growth experiments of α -Ga₂O₃ using a NaOH flux at 4.4 GPa and 1000 °C is only reported. Therefore, we examined the β - α transition pressure at high temperature. The single phase of α -Ga₂O₃, which was transformed from β -Ga₂O₃ at 7.6 GPa and 1500 ± 200 K, was reheated with the pressure changed at intervals. During the decompression process, the diffraction peaks of β -Ga₂O₃ appear between 2.8 and 1.7 GPa at 1200 to 1500 K. Afterward, the β -Ga₂O₃ survived during heating at 3.0 GPa but finally vanished at 3.9 GPa. Considering the hysteresis of compression and decompression, the equilibrium transition boundary is estimated as 2.0 to 3.0 GPa and 1200 to 1500 K. This pressure range is not only consistent with the present computation results (0 GPa) but is also in good agreement with the reported value (2.6 GPa) by another computational method: density functional theory-generalized gradient approximation (DFT-GGA).⁴⁴ The

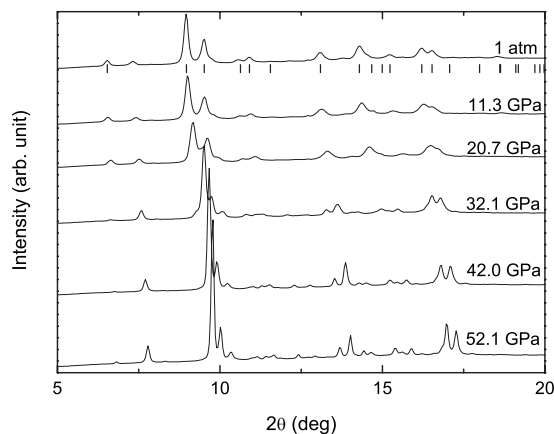


FIG. 6. Variation of x-ray diffraction profiles under decompression on the Rh₂O₃(II) phase in Ga₂O₃. The data were collected by CCD. The Rh₂O₃(II) phase gradually transformed to corundum phase with decreasing pressure at room temperature. Tick marks represent the positions of the diffraction peaks of the corundum phase.

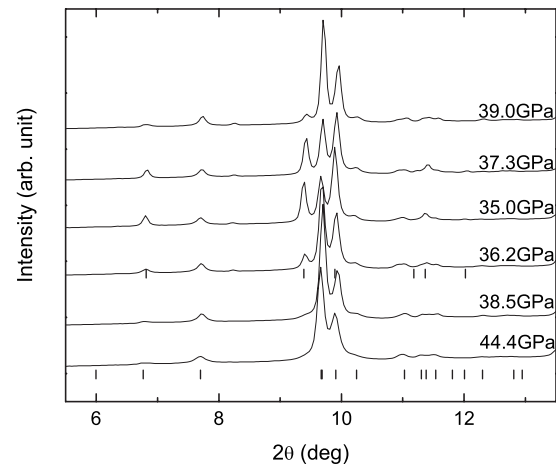


FIG. 7. Variation of x-ray diffraction profiles of Ga₂O₃ phases with changing pressure and temperature. Tick marks represent the positions of the diffraction peaks of the corundum phase (top) and the Rh₂O₃(II) phase (bottom). The data were collected by CCD.

volume-change ratio, $\Delta V = (V_{\beta} - V_{\alpha}) / V_{\beta}$, was calculated to be 7.4% at 3.0 GPa from the present results. As the β -Ga₂O₃ is isomorphous with θ -Al₂O₃,⁴⁵ the 9.2% volume change of θ to α -Al₂O₃ is comparable to that of the present β to α -Ga₂O₃ transition. In terms of the change in oxygen coordination number in gallium, which is from four and six to six, such a large volume change is reasonable for this transition. All experimental conditions and identified phases are summarized in Fig. 8 in order to compare with the primary transition pressure by DFT-LDA computations.

D. Bulk moduli of β , corundum, and Rh₂O₃(II) phases in Ga₂O₃

Corundum is known as one of the hardest oxides and exhibits large bulk modulus ($B_0 = 257$ GPa).⁴⁶ Isostructural α -Ga₂O₃ is therefore expected to indicate a large bulk modu-

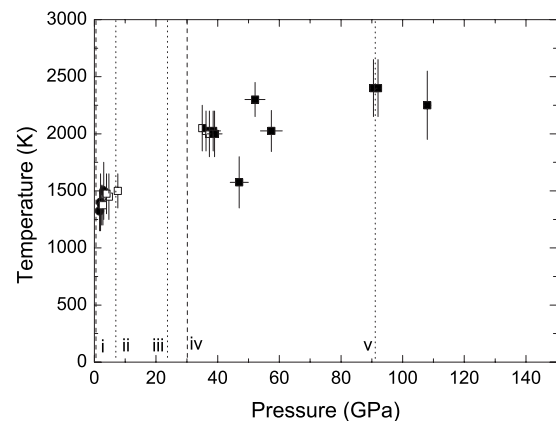


FIG. 8. Data plots of high *P-T* experiments on Ga₂O₃ in comparison with the computation results by DFT-LDA methods. Filled squares, open squares, and filled circles represent Rh₂O₃(II), corundum, and β phase, respectively. Half-filled squares show the observation of the phase mixture of corundum and Rh₂O₃(II). The dotted and broken lines indicate the crossovers by DFT-LDA computations. Notation numbers are the same as those in Fig. 1.

TABLE II. Equation-of-state parameters (B_0 and B'_0) and cell volume per formula unit.

Phase	V_0 (\AA^3)	B_0 (GPa)	B'_0	Method	
Al_2O_3 θ	46.84			XRD (Ref. 45)	
	Corundum	42.51	257 4	XRD (Ref. 46)	
		42.41	240.5 3.94	LDA-GGA (Ref. 21)	
$\text{Rh}_2\text{O}_3(\text{II})$	41.27	261 3.97		LAPW (Ref. 18)	
		261.8 3.93		LDA (Ref. 19)	
Ga_2O_3 β	52.31	134(12)	4	XRD ^a	
	51.14	142	4.1	DFT-LDA ^a	
		202(7)	2.4(6)	XRD (Ref. 11)	
		191(5)	8.3(9)	XRD (Ref. 12)	
	Corundum	~250		XRD(Ref. 11)	
		48.16(4)	223(2)	4	XRD ^a
		47.24	243	4.0	DFT-LDA ^a
	$\text{Rh}_2\text{O}_3(\text{II})$	46.22(22)	271(10)	4	XRD ^a
		45.94	244	4.3	DFT-LDA ^a
	In_2O_3 C-RES	64.78	144(8)	4	XRD ^a
65.13		175	4.5	DFT-LDA ^a	
Corundum		63.05			XRD (Ref. 8)
		63.25	182	3.0	DFT-LDA ^a
$\text{Rh}_2\text{O}_3(\text{II})$		61.75(8)	169(4)	4	XRD ^a
	61.23	192	4.4	DFT-LDA ^a	

^aPresent work.

lus. The bulk moduli of each polymorph calculated from P - V data by least-square fitting to the third-order Birch-Murnaghan equation of state are summarized in Table II. The bulk moduli of α - Ga_2O_3 and $\text{Rh}_2\text{O}_3(\text{II})$ phase are calculated as $B_0=223 \pm 2$ GPa and $B_0=271 \pm 10$ GPa with B'_0 fixed at 4, respectively. Both values are close to the bulk moduli of corundum and $\text{Rh}_2\text{O}_3(\text{II})$ phase in Al_2O_3 . Calculated compression curves are shown together with data points (Fig. 9). By extrapolation, zero pressure volume of $\text{Rh}_2\text{O}_3(\text{II})$ phase can be estimated as 46.22 ± 0.22 \AA^3 per formula unit, where the volume difference between α - Ga_2O_3 and $\text{Rh}_2\text{O}_3(\text{II})$ phase expands by 4.0%. The β - Ga_2O_3 exhibits the much smaller value ($B_0=134 \pm 12$ GPa at $B'_0=4$) than its high-pressure phases. This small value is derived from the existence of gallium with four coordinated oxygen. Relatively large bulk modulus ($B_0=202 \pm 7$ GPa at $B'_0=2.4 \pm 0.6$) is reported by room-temperature compression experiments.¹¹ If the present value is recalculated with B'_0 fixed at 2.4, B_0 only increase by 2 GPa (i.e., $B_0=136 \pm 12$ GPa). Up to 3 GPa, the reported compression curve is almost consistent with our data; thus discrepancy might be attributed to the compression data¹¹ in the metastable pressure region of β - Ga_2O_3 . The static bulk moduli are also obtained by DFT-LDA computations as indicated in Table II. The theoretical values are in reasonable agreement with the experimental values.

E. Phase equilibrium of high-pressure polymorphs in In_2O_3

The present computation results suggest that the transitions for corundum- $\text{Rh}_2\text{O}_3(\text{II})$, C-RES- $\text{Rh}_2\text{O}_3(\text{II})$, and

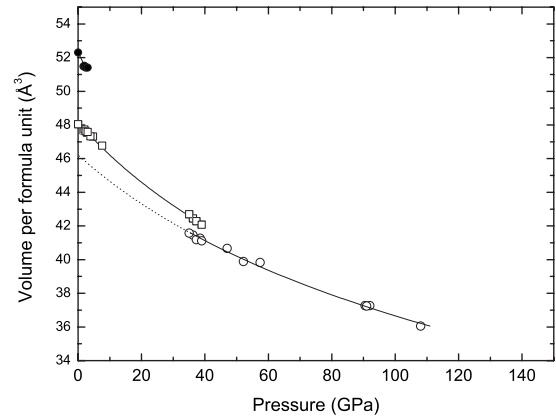


FIG. 9. Pressure-volume data of β phase (solid circles), corundum (open squares), and $\text{Rh}_2\text{O}_3(\text{II})$ (open circles) in Ga_2O_3 . All volume data are normalized per formula unit. The compression curve was obtained by fitting the data to the Birch-Murnaghan equation of state. The dotted curve is extrapolated.

C-RES-corundum would occur around 8 GPa in each case. Accordingly, first the laser-heating experiments were started at pressure less than 10 GPa, as shown in Fig. 10. The C-RES structure with peak broadening still remains after compression to 5.2 GPa. After that, the sample was irradiated by a Nd:YAG laser for a few minutes repeatedly. After the final heating, the pressure was elevated to 8.1 GPa, and the C-RES phase completely changed to $\text{Rh}_2\text{O}_3(\text{II})$ phase. The fitting results by the Rietveld analysis of the $\text{Rh}_2\text{O}_3(\text{II})$ phase are indicated in Fig. 11, and the refined atomic coordinates and the lattice parameters are given in Table III. We note the transient process until the C-RES phase completely disappears. After the first laser heating, the diffraction peaks of $\text{Rh}_2\text{O}_3(\text{II})$ (020), (112), and (200) had already emerged on

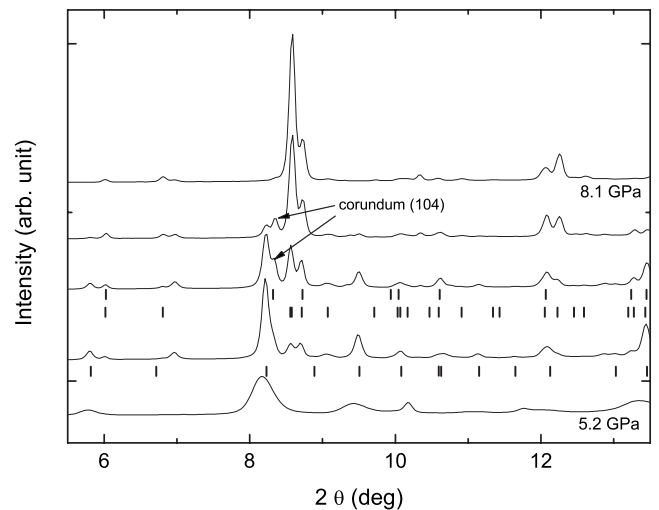


FIG. 10. Variation of x-ray diffraction profiles of In_2O_3 phases with changing pressure and temperature. Tick marks represent the positions of the diffraction peaks of the corundum phase (top), $\text{Rh}_2\text{O}_3(\text{II})$ phase (middle), and the C-RES phase (bottom). The data were collected by CCD.

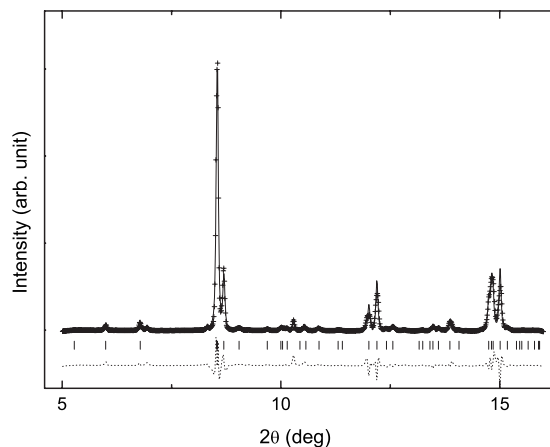


FIG. 11. Powder x-ray diffraction patterns obtained by the Rietveld method (GSAS) for a Rh₂O₃(II) structure in In₂O₃ at 8.1 GPa. The difference (dotted line) between the observed (crosses) and fitted patterns (thin line) is also shown on the same scale. Background was subtracted. Tick marks represent the calculated positions of the diffraction peaks of the Rh₂O₃(II) phase.

the right side of a C-RES (222) peak (Fig. 10). The peaks gradually grew by successive heating. When we carefully examined the diffraction profiles, we temporarily observed a small peak corresponding to corundum (104). Although the pressures in the transient process were not measured at all stages, it seems that the stability field of corundum is limited to be very narrow. This result is consistent with that by computations, except for observation of the limited stability area of corundum phase, which does not exist in the computation results. After decompression, the Rh₂O₃(II) phase could not be quenched at atmospheric pressure and converted to corundum phase as well as the Rh₂O₃(II) phase in Ga₂O₃. In further experiments, the Rh₂O₃(II) phase was confirmed to exist in the pressure range between 8.1 and 19.9 GPa at high temperature. All experimental conditions are plotted in Fig. 12 in comparison with the transition pressure according to the DFT-LDA results. To check the metastability of corundum phase, the quenched products were recompressed to 4.3 GPa and again heated at 1900–2200 K. The diffraction peaks of C-RES phase emerged from the diffraction pattern of corundum structure at 3.0 GPa. It is therefore concluded that the corundum as quenched phase is exactly metastable under

TABLE III. Refined atomic coordinates and lattice parameters determined by Rietveld analysis of the Rh₂O₃(II) phase (*Pbna*; *Z* = 4) in In₂O₃ at 8.1 GPa.

Atom	<i>x</i>	<i>y</i>	<i>z</i>	<i>U</i> _{iso} ^a
In	0.75025	0.02544	0.11587	0.0048
O1	0.60393	0.06094	0.83083	0.0028
O2	0.03027	0.25	0	0.0028
Lattice parameters	<i>a</i> = 5.432 Å	<i>b</i> = 5.539 Å	<i>c</i> = 7.875 Å	<i>R</i> _{wp} = 0.043

^aThe values from corundum-type In₂O₃ (Ref. 8) are used.

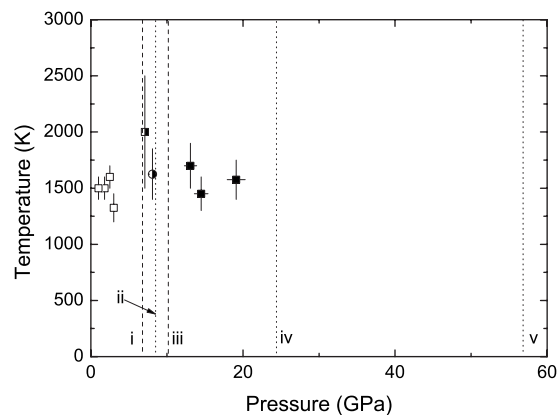


FIG. 12. Data plots of high *P*-*T* experiments on In₂O₃ in comparison with the computation results by DFT-LDA methods. Filled squares and open squares represent Rh₂O₃(II) and C-RES phase, respectively. Half-filled circles represent the observation of the phase mixture of C-RES, Rh₂O₃(II), and corundum phase. Half-filled squares show the observation of the phase mixture of C-RES and Rh₂O₃(II). The dotted and broken lines indicate the crossovers by DFT-LDA computations. Notation numbers are the same as those in Fig. 2.

high pressure. These results are partly inconsistent with the previous reports,¹³ which indicated a small amount of corundum phase in the recovered specimens shocked at 15 to 25 GPa. Although these reports judged the existence of the corundum phase from the quenched products recovered from high-pressure experiments, they could not recognize the Rh₂O₃(II) phase, which was only stable under high pressure. However, in static experiments using a tetrahedral anvil press,^{7,8} it was reported that the C-RES phase is transformed to corundum at 6.5 GPa and 800 to 1300 °C. It is thus so far difficult to conclude that the corundum phase in their experiments is a quenched product from Rh₂O₃(II) phase.

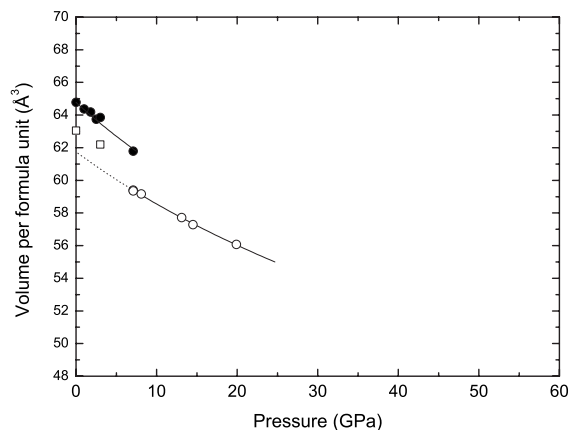


FIG. 13. Pressure-volume data of C-RES (solid circles), corundum (open squares), and Rh₂O₃(II) (open circles) in In₂O₃. All volume data are normalized per formula unit. The compression curve was obtained by fitting the data to the Birch-Murnaghan equation of state. The dotted curve is extrapolated.

F. Volume difference and bulk moduli of polymorphs in In_2O_3

All P - V data are plotted in Fig. 13. The volume difference can be calculated at the pressures where two-phase mixture is observed. At 7.1 GPa, the volume change from C-RES to $\text{Rh}_2\text{O}_3(\text{II})$ phase, $\Delta V = (V_{\text{C-RES}} - V_{\text{Rh}_2\text{O}_3(\text{II})}) / V_{\text{C-RES}}$, is calculated to be 3.9%. If the value is calculated from the volumes extrapolated to atmospheric pressure by the Birch-Murnaghan equation of states, the change expands to 4.7%. Since the volume of corundum phase is located at the intermediate position between C-RES and $\text{Rh}_2\text{O}_3(\text{II})$ phases, the changes, $\Delta V = (V_{\text{C-RES}} - V_{\text{corundum}}) / V_{\text{C-RES}}$, and $\Delta V = (V_{\text{corundum}} - V_{\text{Rh}_2\text{O}_3(\text{II})}) / V_{\text{corundum}}$ are calculated to be 2.7 and 2.1%, respectively. The latter change is significantly smaller than the isomorphous volume changes in Ga_2O_3 described above. The bulk modulus of C-RES and $\text{Rh}_2\text{O}_3(\text{II})$ phase was calculated as 144 ± 8 GPa and 169 ± 4 GPa, respectively, as shown in Table II. As well as the gallia's cases, these values are also consistent with theoretical values of 175 GPa and 191 GPa produced from the DFT-LDA calculations. Note that at 300 K, temperature and zero-point vibration effects usually depress bulk modulus by $\sim 10\%$. As compared to $\text{Rh}_2\text{O}_3(\text{II})$ phase in Al_2O_3 , and Ga_2O_3 , the bulk modulus of $\text{Rh}_2\text{O}_3(\text{II})$ phase in In_2O_3 exhibits rather a small value. This is in accordance with the prediction of Majewski and Vogl,⁴⁷ suggesting that the bulk modulus decreases with increasing unit-cell volume. This $B_0 - V$ relation is also typically shown in type IIIB nitrides phases, such as AlN, GaN, and InN, where the bulk moduli of InN exhibits the smallest values among them.^{48,49}

G. Perspective on post $\text{Rh}_2\text{O}_3(\text{II})$ phase

It is well known that the crystal structure of the sesquioxides is correlated with cation size, as typically shown in the rare-earth sesquioxides.²⁴ Since the ratio of cation and anion sizes varies with pressure, the structure sequentially changes from C to B or A-RES structure with increasing pressure. In case of In_2O_3 and Tl_2O_3 , belonging to type IIIB sesquioxides, the corundum structure appears as a next phase of C-RES structure.⁸ On the basis of cation coordination and density increase, the phase sequence $\text{C} \rightarrow \text{corundum} \rightarrow \text{B}$ was proposed at that time.⁸

Considering the volume-reduction ratio from C to B-RES phase, the volume reduction is assumed to be 8%, as the coordination of cations in the B-RES structure is closer to seven than six.⁸ In the present experiments on In_2O_3 , the C-RES- $\text{Rh}_2\text{O}_3(\text{II})$ transition exhibits only 3.9% volume re-

duction at the transition pressure. This value is much smaller than 8%, which is expected in the C-B-RES transition. Despite further compression of $\text{Rh}_2\text{O}_3(\text{II})$ phase, yielding a volume reduction of more than 4%, the B-RES phase did not appear. This result might predict a higher oxygen-coordinated phase than B-RES as the post $\text{Rh}_2\text{O}_3(\text{II})$ phase in In_2O_3 .

A similar consideration can be applicable to the post- $\text{Rh}_2\text{O}_3(\text{II})$ phase in Ga_2O_3 . If C-RES phase exists prior to the corundum- $\text{Rh}_2\text{O}_3(\text{II})$ transition in Ga_2O_3 , and the volume change ($\Delta V = 2.4\%$) is assumed as well as In_2O_3 , at least 4.7% would be estimated for the volume reduction of the C-RES- $\text{Rh}_2\text{O}_3(\text{II})$ transition. This volume change is also within 8%, so the appearance of $\text{Rh}_2\text{O}_3(\text{II})$ prior to B-RES phase has no contradiction in density. It is surprising that a new phase was not found even after compression to 108 GPa, where 13% volume reduction was observed. The post $\text{Rh}_2\text{O}_3(\text{II})$ phase in Ga_2O_3 would therefore exhibit a different structure from B-RES. We will report on the further structural evolution of Ga_2O_3 beyond 110 GPa in a subsequent paper.⁴¹

IV. SUMMARY

New $\text{Rh}_2\text{O}_3(\text{II})$ structures in Ga_2O_3 and In_2O_3 , in addition to Al_2O_3 , Fe_2O_3 , and Rh_2O_3 , were found. These $\text{Rh}_2\text{O}_3(\text{II})$ structures converted to corundum structure at ambient pressure. The results of Rietveld refinements and DFT-LDA computations gave negative evidence for the presence of orthorhombic perovskite structures as their postcorundum phase. Contrary to the previous study, the stability area of corundum phase in In_2O_3 was confirmed to be very limited. Considering the similarity between corundum and $\text{Rh}_2\text{O}_3(\text{II})$ structure, an appearance of the $\text{Rh}_2\text{O}_3(\text{II})$ phase prior to a transition involving coordination change is quite reasonable in regard to type IIIB sesquioxides.

ACKNOWLEDGMENTS

The synchrotron radiation experiments were performed at the BL-10XU in SPring-8 with the approval of the Japan Synchrotron Radiation Research Institute (JASRI) (Proposal Nos. 2006A1154 and 2006B1121). H.Y. acknowledges support from NIMS Exploratory Research Funds. T.T. acknowledges support from Ehime Univ. Project Fund and Grant-in-Aid for Scientific Research from the Japan Society for the Promotion of Science (Nos. 18840033 and 19740331).

*yusa.hitoshi@nims.go.jp

†takut@sci.ehime-u.ac.jp

‡sata@jamstec.go.jp

§ohishi@spring8.or.jp

¹N. Ueda, H. Hosono, R. Waseda, and H. Kawazoe, *Appl. Phys. Lett.* **70**, 3561 (1997).

²K. Matsuzaki, H. Yanagi, T. Kamiya, H. Hiramatsu, K. Nomura,

M. Hirano, and H. Hosono, *Appl. Phys. Lett.* **88**, 092106 (2006).

³C. G. Granqvist, *Appl. Phys. A: Solids Surf.* **A57**, 19 (1993).

⁴H. Mizoguchi and P. M. Woodward, *Chem. Mater.* **16**, 5233 (2004).

⁵J. P. Remeika and M. Marezio, *Appl. Phys. Lett.* **8**, 87 (1966).

⁶M. Marezio and J. P. Remeika, *J. Chem. Phys.* **46**, 1862 (1967).

- ⁷R. D. Shannon, *Solid State Commun.* **4**, 629 (1966).
- ⁸C. T. Prewitt, R. D. Shannon, D. B. Rogers, and A. W. Sleight, *Inorg. Chem.* **8**, 1985 (1969).
- ⁹T. P. Beales, C. H. L. Goodman, and K. Scarrott, *Solid State Commun.* **73**, 1 (1990).
- ¹⁰B. Tu, Q. Cui, P. Xu, X. Wang, W. Gao, C. Wang, J. Liu, and G. Zou, *J. Phys.: Condens. Matter* **14**, 10627 (2002).
- ¹¹D. Machon, P. F. McMillan, B. Xu, and J. Dong, *Phys. Rev. B* **73**, 094125 (2006).
- ¹²K. E. Lipinska-Kalita, B. Chen, M. B. Kruger, Y. Ohki, J. Murowchick, and E. P. Gogol, *Phys. Rev. B* **68**, 035209 (2003).
- ¹³T. Atou, K. Kusaba, K. Fukuoka, M. Kikuchi, and Y. Syono, *J. Solid State Chem.* **89**, 378 (1990).
- ¹⁴M. Epifani, P. Siciliano, A. Gurlo, N. Barsan, and U. Weimar, *J. Am. Chem. Soc.* **126**, 4078 (2004).
- ¹⁵D. Yu, D. Wang, and Y. Qian, *J. Solid State Chem.* **177**, 1230 (2004).
- ¹⁶M. Sorescu, L. Diamandescu, D. Tarabasanu-Mihaira, and V. S. Teodorescu, *J. Mater. Sci.* **39**, 675 (2004).
- ¹⁷H. Cynn, D. G. Isaak, R. E. Cohen, M. F. Nicol, and O. L. Anderson, *Am. Mineral.* **75**, 439 (1990).
- ¹⁸F. C. Marton and R. E. Cohen, *Am. Mineral.* **79**, 789 (1994).
- ¹⁹K. T. Thomson, R. M. Wentzcovitch, and M. S. T. Bukowinski, *Science* **274**, 1880 (1996).
- ²⁰W. Duan, R. M. Wentzcovitch, and K. T. Thomson, *Phys. Rev. B* **57**, 10363 (1998).
- ²¹J. Tsuchiya, T. Tsuchiya, and R. M. Wentzcovitch, *Phys. Rev. B* **72**, 020103(R) (2005).
- ²²N. Funamori and R. Jeanloz, *Science* **278**, 1109 (1997).
- ²³J. F. Lin, O. Degtyareva, C. T. Prewitt, P. Dera, N. Sata, E. Gregoryanz, H. K. Mao, and R. J. Hemley, *Nat. Mater.* **3**, 389 (2004).
- ²⁴A. F. Wells, *Structural Inorganic Chemistry*, 5th ed. (Clarendon Press, Oxford, 1984).
- ²⁵M. P. Pasternak, G. K. Rozenberg, G. Y. Machavariani, O. Naaman, R. D. Taylor, and R. Jeanloz, *Phys. Rev. Lett.* **82**, 4663 (1999).
- ²⁶G. K. Rozenberg, L. S. Dubrovinsky, M. P. Pasternak, O. Naaman, T. LeBihan, and R. Ahuja, *Phys. Rev. B* **65**, 064112 (2002).
- ²⁷S. Ono, T. Kikegawa, and Y. Ohishi, *J. Phys. Chem. Solids* **65**, 1527 (2004).
- ²⁸S. Ono, K. Funakoshi, Y. Ohishi, and E. Takahashi, *J. Phys.: Condens. Matter* **17**, 269 (2005).
- ²⁹T. Watanuki, O. Shimomura, T. Yagi, T. Kondo, and M. Isshiki, *Rev. Sci. Instrum.* **72**, 1289 (2001).
- ³⁰T. Kurashina, K. Hirose, S. Ono, N. Sata, and Y. Ohishi, *Phys. Earth Planet. Inter.* **145**, 67 (2004).
- ³¹A. P. Hammersley, FIT2D: An Introduction and Overview, European Synchrotron Radiation Facility Internal Report No. ESRF97HA02T, 1997, http://www.esrf.eu/computing/scientific/FIT2D/FIT2D_INTRO/fit2d.html
- ³²H. K. Mao, P. M. Bell, J. W. Shaner, and D. J. Steinberg, *J. Appl. Phys.* **49**, 3276 (1978).
- ³³J. C. Jamieson, J. N. Fritz, and M. H. Manghnani, *High-Pressure Research in Geophysics* (Center for Academic Publication Japan, Tokyo, 1982), pp. 27–48.
- ³⁴P. Hohenberg and W. Kohn, *Phys. Rev.* **136**, B864 (1964).
- ³⁵D. M. Ceperley and B. J. Alder, *Phys. Rev. Lett.* **45**, 566 (1980).
- ³⁶J. P. Perdew and A. Zunger, *Phys. Rev. B* **23**, 5048 (1981).
- ³⁷D. Vanderbilt, *Phys. Rev. B* **41**, 7892 (1990).
- ³⁸H. J. Monkhorst and J. D. Pack, *Phys. Rev. B* **13**, 5188 (1976).
- ³⁹R. M. Wentzcovitch, *Phys. Rev. B* **44**, 2358 (1991).
- ⁴⁰<http://www.pwscf.org>
- ⁴¹T. Tsuchiya, H. Yusa, and J. Tsuchiya, *Phys. Rev. B* **76**, 174108 (2007).
- ⁴²R. D. Shannon and C. T. Prewitt, *J. Solid State Chem.* **2**, 134 (1970).
- ⁴³A. C. Larson and R. B. Von Dreele, General Structure Analysis System (GSAS). Report LAUR 86–748. Los Alamos National Laboratory, New Mexico, 2004, <http://www.ccp14.ac.uk/ccp/ccp14/ftp-mirror/gsas/public/gsas/manual/GSASManual.pdf>
- ⁴⁴P. Kroll, *Phys. Rev. B* **72**, 144407 (2005).
- ⁴⁵S. J. Wilson and J. D. C. M. Connell, *J. Solid State Chem.* **34**, 315 (1980).
- ⁴⁶L. W. Finger and R. M. Hazen, *J. Appl. Phys.* **49**, 5823 (1978).
- ⁴⁷J. A. Majewski and P. Vogl, *Phys. Rev. B* **35**, 9666 (1987).
- ⁴⁸M. Ueno, M. Yoshida, A. Onodera, O. Shimomura, and K. Takemura, *Phys. Rev. B* **49**, 14 (1994).
- ⁴⁹J. Serrano, A. Rubio, E. Hernandez, A. Munoz, and A. Mujica, *Phys. Rev. B* **62**, 16612 (2000).